Ruhr-Universität Bochum, SS 2019

Fortgeschrittenen-Praktikum Theorie

Numerical Simulation of Cardiac Tissue Electrophysiology

Jeremiah Lübke, 108015230366

July 20, 2019
Advisor: Dr. Jürgen Dreher

Contents

1. Introduction

The human heart is a fascinating apparatus, which does its work in a constant and reliable fashion – usually without disruption – for the whole of a persons life. To put things into perspective, the heart of an average human being performs

	70	typical rest pulse per minute
$\times$	1440	minutes per day
$\times$	365	days per year
$\times$	80	estimated average human life time
$\sim$	$\mathbf{3 \times 10^9}$	**beats per life time**,

while a typical car engine performs

	300 000	km driven during the cars life time
/	50	average speed in km/h
$\times$	60	minutes per hour
$\times$	2200	typical revolutions per minute
$\sim$	$\mathbf{8 \times 10^8}$	**duty cycles per life time**.

Investigating the hearts physical working principle poses an interesting challenge with undoubtedly many relevant applications such as gaining a deeper understanding of and developing more advanced treatments for often dangerous arrhythmia.

The heart muscles basic functionality is rhythmically contracting itself triggered by electrical signals, which are being conducted by the heart muscle cells (the cardiomyocytes) themselves: the cardiac tissue combines the ability to both perform mechanical work and conduct electrical signals. This is very remarkable, because usually these tasks are separately taken care of by muscle and neural cells, respectively.

Going a little more into detail: pacemaker cells (specialized cardiomyocytes) in the SA-node rhythmically generate action potentials which travel at about 0.05 to $1\,\mathrm{m\,s^{-1}}$ to the AV-node and from there after a delay at about 2 to $4\,\mathrm{m\,s^{-1}}$ through the His and ventricular bundles and the Purkinje fibres, eventually reaching the intended tissue and causing its contraction.

1.1. Structure of the Cardiomyocytes

For a better understanding it is helpful to take a closer look at the microscopic structure of the cardiomyocytes:

Cardiomyocytes are tubular cells, which are enclosed by the *sarcolemma* (a double lipid-layered membrane) and contain chains of *myofibril* (fibres composed of long proteins), which are responsible for contraction of the muscle tissue. Additionally the cells contain the *sarcoplastic reticulum*, which is a membrane-enclosed region, mainly for storing Ca^{2+} ions.

In longitudinal direction *interlacing disks* join the cells together and via the *gap junctions* allow propagation of action potentials. Because of these features the heart muscle forms a *syncytium*, i. e. the whole of the single cells behaves like a single coordinated unit.

1.2. Modeling the membrane potential

Now the interior and exterior (i. e. the intermediate space between neighbouring cells) regions of a cells exhibit different concentrations of various ion species (this imbalance is being maintained by specialized ion pumps and gates in the cell membrane), which results in a voltage between those regions: the membrane potential $V = \Phi_i - \Phi_e$, which in the rest case is equal to some rest potential V_{rest}.

If at some point the membrane potential is perturbed by a stimulus in such a way that it exceeds some threshold, the ion channels rapidly open causing the concentration difference of the ions between

interior and exterior cell regions to invert resulting in a large upswing of the membrane potential. This process is called *depolarization* and the peak of the membrane potential is called *action potential*. After reaching this peak the gates close again and the pumps recreate the prior concentration difference which causes the membrane potential to return to the rest value (*repolarization*).

Since the membrane posses a finite specific electric capacity $C\,[\mathrm{F\,m^{-2}}]$, the membrane potential obeys the capacitor equation:

$$I = C\,\frac{\mathrm{d}V}{\mathrm{d}t} = -\sum_s I_s \tag{1}$$

were the total membrane current density I is the sum of all involved species-specific current densities. Therewith the dynamics of V can be modeled by modeling the membrane current densities I_s.

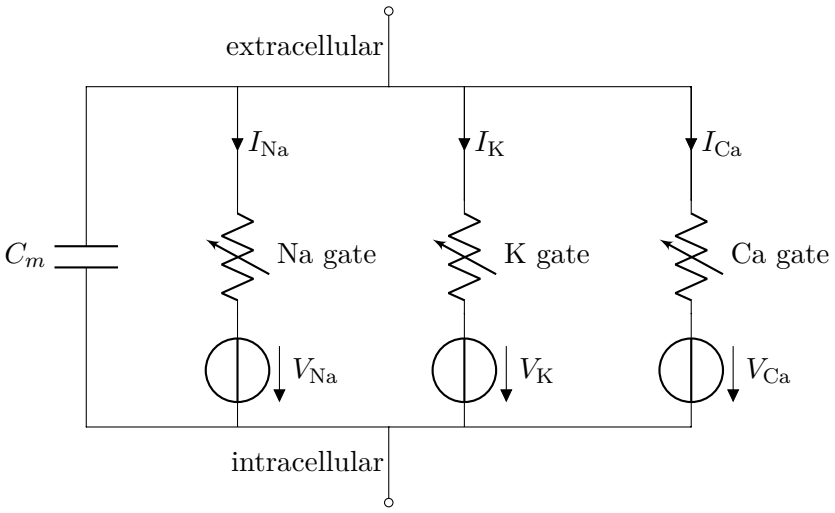

Figure 1: Example of an electrical circuit representing the membrane structure

1.3. Developing a Continuum Description

At a microscopic level the propagation of action potential is a discrete process (from cell to cell). However looking at tissue at sufficiently large scales, it can be viewed as continuous ($\rightarrow$ *functional syncytium*). It is important to note the anisotropic nature of this process: the tissue exhibits different conductivities in longitudinal and transversal direction with respect to the myofibril.

1.3.1. Bidomain model

One formulates potentials Φ_i, Φ_e and current densities $\mathbf{J_i}, \mathbf{J_e}$ for the intra- and extracellular regions. It is important to note, that formally all of these functions are defined on the whole domain.

To set them into relation, consider Possion's equation and Ohm's Law:

$$\mathbf{E} = -\nabla\Phi, \quad \mathbf{J} = \mathbf{G}\,\mathbf{E}$$
$$\implies \mathbf{J_i} = -\mathbf{G_i}\,\nabla\Phi_i, \quad \mathbf{J_e} = -\mathbf{G_e}\,\nabla\Phi_e$$

where $\mathbf{E}$ is the electrical field associated with the potential Φ and $\mathbf{G}$ is the conductivity tensor accounting for the anisotropy.

Imposing conservation of current:

$$\nabla\cdot(\mathbf{J_i}+\mathbf{J_e}) = 0 \implies -\nabla\cdot\mathbf{J_i} = \nabla\cdot\mathbf{J_e} = I_m$$

(where I_m is the transmembrane current density with units $\mathrm{A\,m^{-3}}$), and rewriting the capacitor equation (1):

$$I_m = \beta\left(C\,\frac{\partial V}{\partial t} + \sum_s I_s\right), \quad V = \Phi_i - \Phi_e$$

(where β is a scaling constant with units m^{-1}), one finds after some calculations:

$$\nabla \cdot \mathbf{G_i}(\nabla V + \nabla \Phi_e) = \beta \left(C \frac{\partial V}{\partial t} + I_{\text{ion}} \right) \tag{2a}$$

$$\nabla \cdot ((\mathbf{G_i} + \mathbf{G_e}) \nabla \Phi_e) = -\nabla \cdot (\mathbf{G_i} \nabla V) \tag{2b}$$

Now one has a system of two coupled PDEs with (2a) being parabolic and (2b) being elliptic, which is rather difficult to solve.

1.3.2. Monodomain model

In order to make matters more accessible, one makes the assumption that the intra- and extracellular anisotropies are identical, i. e. the respective conductivities are proportional:

$$\mathbf{G_e} = \lambda \mathbf{G_i}$$

$$\implies \frac{\partial V}{\partial t} = \nabla \cdot \mathbf{D} \nabla V - \frac{1}{C} \sum_s I_s \tag{3}$$

(with the conductivity tensor $\mathbf{D} = \frac{1}{C\beta}\mathbf{G}$) which reduces the problem to one parabolic PDE (a diffusion equation).

Now all that is left to do is to model the conductivity tensor $\mathbf{D}$ to represent the tissue at hand. One way of doing this is to split this object into components parallel and perpendicular to the direction of the myofibril $\mathbf{f}$, like so

$$\mathbf{D} = \mathbf{D}_\perp \mathbb{1} + (\mathbf{D}_\parallel - \mathbf{D}_\perp) \mathbf{f}\, \mathbf{f}^{\mathbf{T}}$$

where for typical cardiomyocytes one has the relation $D_\parallel / D_\perp \sim 2 \ldots 10$.

Another way is to neglect the anisotropies all together and write the conductivity tensor as a scalar value: $\mathbf{D} \to \eta$. This is the approach taken by the following investigations.

Note: Without external stimuli (enforced by von Neumann boundary conditions) bi- and monodomain models yield almost identical results. However when considering such external stimuli (e. g. defibrillation) the unequal anisotropies of intra- and extracellular regions are significant.

2. Three Models

This section is going to describe three approaches – out of an abundance of available models (`www.cellml.org`) – which can be used to describe the dynamics of the membrane potential.

2.1. Hodgkin & Huxley (1952)

This model was developed by A. L. Hodgkin and A. F. Huxley to fit measurements taken on a giant squid axon prior to detailed knowledge about the biophysical mechanisms being available.

The membrane current density in (1) is modeled as the sum of Sodium, Potassium and a leakage current, each obeying Ohm's Law:

$$I_m = \sum_s I_s = I_{\text{Na}} + I_{\text{K}} + I_{\text{leak}}$$

$$I_s = g_s (V - V_s)$$

where the specific conductivites are described by dimensionless gating variables $n, m, h \in [0, 1]$:

$$g_{\text{Na}} = \bar{g}_{\text{Na}}\, n^4, \quad g_{\text{K}} = \bar{g}_{\text{K}}\, m^3\, h, \quad g_{\text{leak}} = \bar{g}_{\text{leak}}$$

The respective rest potentials and maximal specific conductivities were measured as:

Current	V_s/mV	$\bar{g}_s$/mS cm^{-2}
Na	115	120
K	−12	36
leak	10	0.3

And the gating variables obey the following ODEs:

$$\frac{\mathrm{d}n}{\mathrm{d}t} = \alpha_n\,(1-n) - \beta_n \tag{4a}$$

$$\frac{\mathrm{d}m}{\mathrm{d}t} = \alpha_m\,(1-m) - \beta_m \tag{4b}$$

$$\frac{\mathrm{d}h}{\mathrm{d}t} = \alpha_h\,(1-h) - \beta_h \tag{4c}$$

with ($\tilde{V} = V/\mathrm{mV}$):

$$\alpha_n = 0.01\,\mathrm{ms}^{-1}\frac{\tilde{V}-10}{1-\exp\left(\frac{10-\tilde{V}}{10}\right)}, \qquad \beta_n = 0.125\,\mathrm{ms}^{-1}\exp\left(-\frac{\tilde{V}}{80}\right)$$

$$\alpha_m = 0.1\,\mathrm{ms}^{-1}\frac{\tilde{V}-25}{1-\exp\left(\frac{25-\tilde{V}}{10}\right)}, \qquad \beta_m = 4\,\mathrm{ms}^{-1}\exp\left(-\frac{\tilde{V}}{18}\right)$$

$$\alpha_h = 0.07\,\mathrm{ms}^{-1}\exp\left(-\frac{\tilde{V}}{20}\right), \qquad \beta_h = \frac{1}{1+\exp\left(\frac{30-\tilde{V}}{10}\right)}$$

Thus, one has to solve a system of four first-order uncoupled ODEs (1, 4a, 4b, 4c).

2.2. Aliev & Panfilov (1996)

While the Hodkin-Huxley model gives a very good description of action potential dynamics, it is rather complex and therefor not preferable for large scale computations.

An alternative model was formulated by Aliev and Panfilov, which refrains from using a description based on biophysical details and instead uses two variables (the potential V and a relaxation variable W) to phenomenologically reproduce the membrane potential dynamics of cardiomyocytes:

$$\frac{\mathrm{d}V}{\mathrm{d}t} = -k\,V\,(V-a)\,(V-1) - V\,W \tag{5a}$$

$$\frac{\mathrm{d}W}{\mathrm{d}t} = \epsilon(V,W)\,(-k\,V\,(V-a-1) - W) \tag{5b}$$

$$\epsilon = \epsilon_0 + \frac{\mu_1\,W}{V+\mu_2}$$

The relaxation variable W summarizes (or hides) all the complex processes involving ion pumps etc., which cause the membrane potential to repolarize.

Here one has to solve two coupled first-order ODEs.

2.3. Fenton et al (2002)

Yet another model to be introduced here is again based on the capacitor equation (1). Unlike the models presented above, this approach allows to easily investigate chaotic wave breakup mechanisms (its technical meaning and possible physiological interpretation will be discussed in section 4.2 and section 5, respectively).

The membrane current density is modeled as the sum of the following phenomenological current densities:

- fast inward current
$$I_{fi} = -v\,\Theta(V - V_c)\,(V - V_c)\,(1 - V)/\tau_d$$
  - depolarizes membrane upon an excitation above V_c
  - depends on a fast activation mechanism $\Theta(V - V_c)$ modeled by a Heaviside step function and the fast inactivation gate v
- slow outward current
$$I_{so} = V\,(1 - \Theta(V - V_c))/\tau_0 + \Theta(V - V_c)/\tau_r$$
  - repolarizes membrane back to resting potential
  - depends on fast activation mechanism $\Theta(V - V_c)$
- slow inward current
$$I_{si} = -w\,\frac{d}{2\,\tau_{si}}, \quad d \to 1 + \tanh\big(k\,(V - V_c^{si})\big)$$
  - inactivation current to balance I_{so}
  - produces observed plateau in action potential
  - depends on slow inactivation gate w and on a very fast activation gate d, which is modeled by a steady-state function

The two gate variables governing the currents:

- fast inactivation gate
$$\frac{\mathrm{d}v}{\mathrm{d}t} = (1 - \Theta(V - V_c))\,(1 - v)/\tau_{v-} - \Theta(V - V_c)\,v/\tau_{v+} \tag{6}$$
$$\text{with} \quad \tau_{v-} = (1 - \Theta(V - V_v))\,\tau_{v-,1} + \Theta(V - V_v)\,\tau_{v-,2}$$
- slow inactivation gate
$$\frac{\mathrm{d}w}{\mathrm{d}t} = (1 - \Theta(V - V_c))\,(1 - w)/\tau_{w-} - \Theta(V - V_c)\,w/\tau_{w+} \tag{7}$$

And finally the parameters:

- $\tau_{v+}, \tau_{v-,1}, \tau_{v-,2}$: opening (+) and closing (–) times of the fast variable v
- τ_{w+}, τ_{w-}: opening and closing times of the slow variable w
- τ_d, τ_r: de- and repolarization times
- τ_0, τ_{si}: time constants for slow currents
- V_c, V_v, V_c^{si}: voltage thresholds
- k: activation width parameter

The problem to be solved here is composed of three uncoupled first-order ODEs (1, 6, 7).

3. Dynamics of a Single Cell

In this section the results of the numerical solutions for a single cell using the three models presented above are discussed. All results were obtained with a simple Forward-Euler scheme.

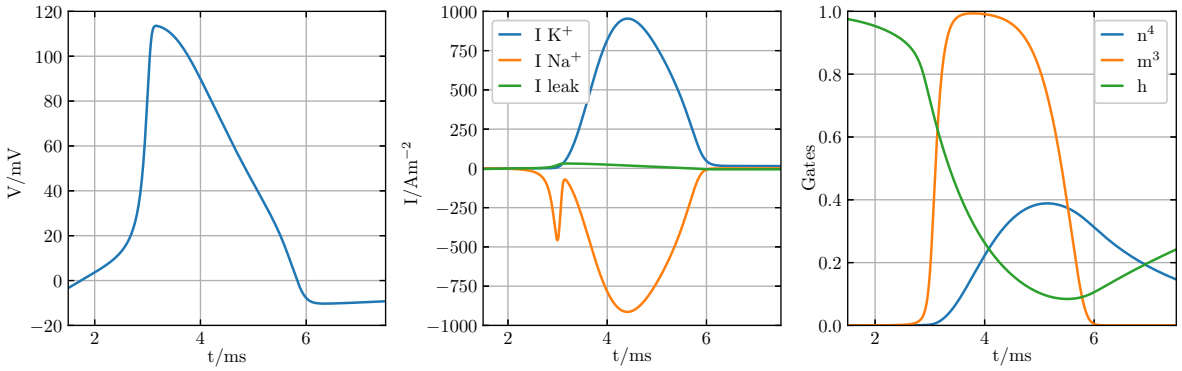

(a) Potential (b) Current Densities (c) Gating Variables

Figure 2: Results of integrating the H&H model

3.1. Hodgkin & Huxley

The equations were integrated for 10 ms with a time step $\Delta t = 0.01$ ms (i. e. 1000 integrations steps) and an initial potential $V_0 = -7$ mV. The resulting action potential, current densities and gating variables are plotted in fig. 2.

The gating variables were initially all set to 0, yet at $t = 0$ ms the Na^+ gate h jumps directly to being almost completely open ($h(t = 0) = 0.99$); however, the Na^+ current is at this point suppressed by the closed m gate. The h gate slowly closes up to $t \approx 5$ ms and then swings down more rapidly, while at the same time the m gate opens strongly and allows for influx of Na^+ ions (interestingly the Na^+ current exhibits a small seperate peak at $t \approx 5$ ms before rising up to its full strength). This causes the membrane potential to rise up and become strongly positive. Shortly after the quick opening of the m gate, the K^+ gate n also opens, allowing for an opposed K^+ outflux causing the membrane potential to eventually repolarize.

The resulting action potential resembles qualitatively the results depicted in fig. 12 in [HH52]. An even better fit is achieved when integrating the system for 40 ms with and initial value of $V_0 = -30$ mV, as depicted in fig. 22 in [HH52] (see fig. 3).

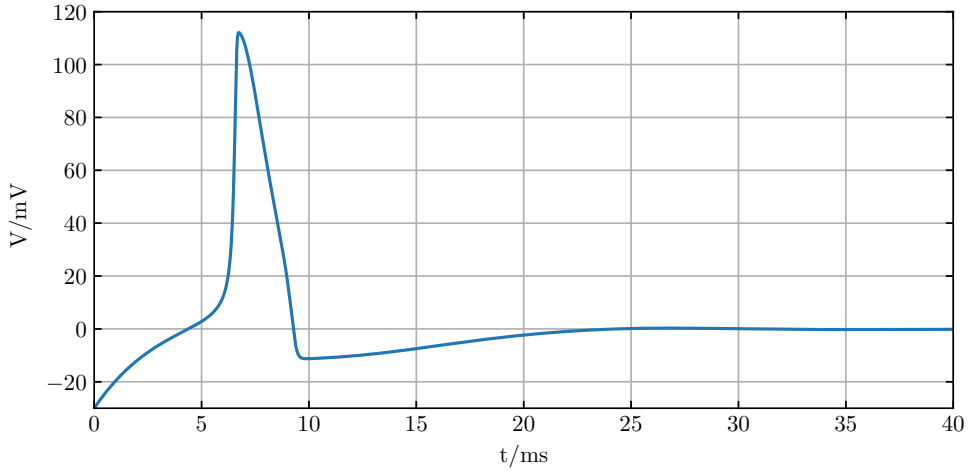

Figure 3: H&H for 40 ms; note the hyperpolarization

Another interesting effect can be observed when adding an additional source current density to equation (1), i. e.:

$$C \frac{\mathrm{d}V}{\mathrm{d}t} = -\sum_s I_s + I_{\text{source}}$$

which causes the membrane potential to depolarize again after repolarization with a constant rate as depicted in fig. 4. Note, that the cell is firing with a fixed minimal rate given by I_{source} (All-or-None principle).

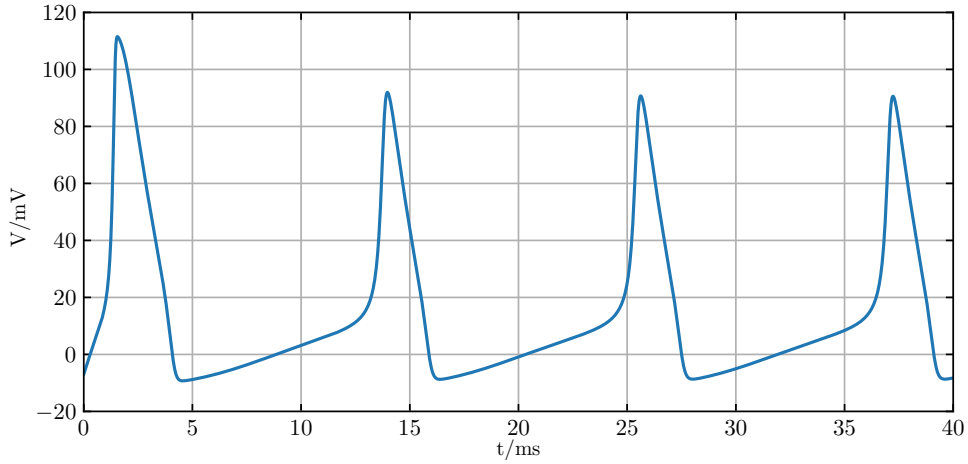

Figure 4: H&H with $I_{\text{source}} = 10\,\text{A}\,\text{m}^{-2}$

3.2. Aliev & Panfilov

Note: The action potential V in this model takes values in $(0, 1)$ and needs to be rescaled according to $V_{\text{phys}}/\text{mV} = 100\,V - 80$. The simulation time t is related to the physical time via $t_{\text{phys}}/\text{ms} = 12.9\,t$.

The integration was performed for 60 stu (simulationt time units, i. e. $t_{\text{phys}} = 774\,\text{ms}$) with a time step of $\Delta t = 0.01\,\text{stu}$, resulting in 6000 integration steps and an initial excitement of the potential to $V_0 = 0.2\,\text{svu}$ (simulation voltage units, i. e. $V_{\text{phys},0} = -60\,\text{mV}$).

Upon an excitement which surpasses some threshold, the action potential quickly raises up to its maximal value and decreases rather weakly at first, thus forming a plateau. The relaxation variable begins raising, too, slowly at first, but gradually growing faster until it steeply reaches its peak, which pulls the action potential back to its resting value.

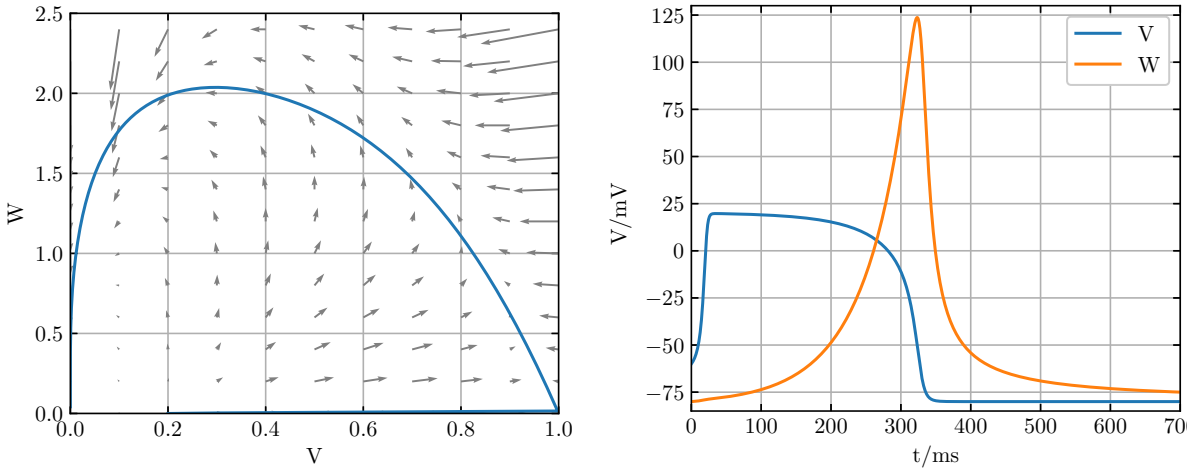

(a) Phase plot of the system, shows the characteristic connection of the two variables (unscaled)

(b) Temporal evolution of the two variables (physically rescaled)

Figure 5: Results of integrating the A&P model

The model dynamics are governed by a set of five parameters a, k, ϵ_0, μ_1 and μ_2. They are phe-

nomenological in their nature and therefor difficult to interpret. A quick study which varies each parameter while holding the others constant is found in the appendix (A.1).

3.3. Fenton et al

Note: In this model the action potential also takes values in $(0, 1)$ and needs to be rescaled with $V_{\text{phys}}/\text{mV} = 100\,V - 80$; however, the simulation time closely resembles the physical time.

The integration was performed for 400 ms using a time step $\Delta t = 0.1$ ms (resulting in 4000 integration steps) and an initial excitement of the potential $V_0 = 0.3$ stu (i. e. $V_{\text{phys}} = -50$ mV).

The resulting action potential qualitatively resembles the result from the Aliev-Panfilov model, with the difference that the peak does not start decreasing right after the excitement but rather shows a slight bump in the plateau. Just like the Hodgkin-Huxley model, the Fenton model is based on an ionic description, which allows to comprehend the action potential dynamics based on underlying gate and current processes.

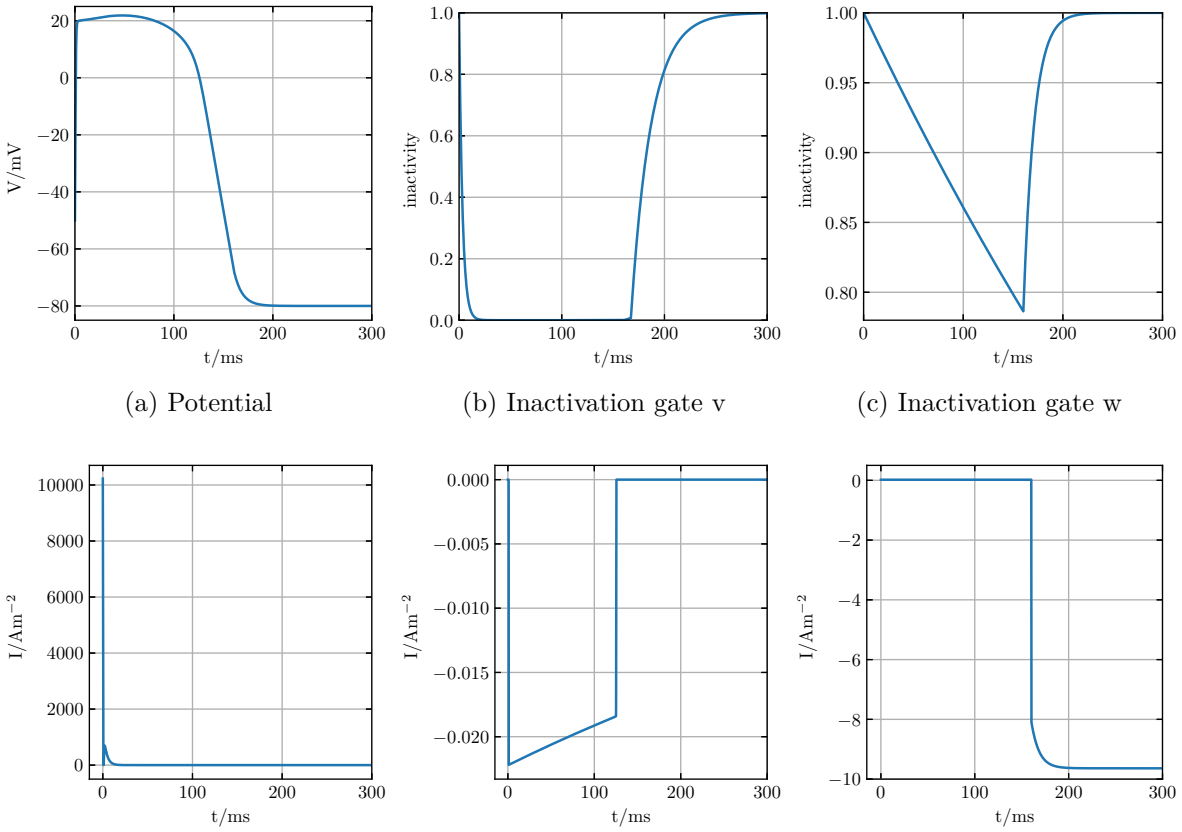

(a) Potential (b) Inactivation gate v (c) Inactivation gate w

(d) fast inward current (e) slow inward current (f) slow outward current

Figure 6: Results of integrating the Fenton model

Here are a few things to note:

- the gate variables are *inactivation gates*, i. e. 1 means fully closed, while 0 means fully opened
- while the fast inactivation gate v opens completely upon excitement and then returns into its closed state, the slow inactivation gate w does not open completely (only ca. 21%) before closing again rather quickly.
- the currents are modeled with Heaviside-functions in order to be activated at once when the potential surpasses a certain threshold (given by the parameters V_c and V_v); this causes the sudden jumps in the plots of the current densities

4. Continuous Spatial Dynamics

The spatial tissue simulations discussed in this section are based on a continuous approximation of the tissue, which in reality is composed of discrete cells. The mathematical approach was introduced in section 1.3. In practice – regardless of the specific model used – one adds a diffusion term to the ODE describing the temporal evolution of the membrane potential and obtains a parabolic PDE:

$$\frac{\partial V}{\partial t} = G(V) \longrightarrow \frac{\partial V}{\partial t} = \eta \nabla^2 V + G(V)$$

In this case the – usually anisotropic – diffusivity is given by the scalar coefficient η, which was set to $\eta = 0.3$ in all cases presented below. Additionally, the time step is computed in each case to fulfill the CFL condition:

$$\Delta t < \frac{(\Delta x)^2}{2\,\eta}$$

4.1. On a one-dimensional domain

The simulation was performed using the Aliev-Panfilov model. For the calculations two one-dimensional arrays were used, representing the values of the membrane potential and the relaxation variable along a discretized line, the length of which has been varied throughout the simulations while holding the grid spacing constant at $\Delta x = 0.2$.

At the beginning von-Neumann boundary conditions were imposed and the first value of the potential array was set to one. Then at each time step both arrays were updated using a simple Euler scheme according to

$$\frac{\partial V}{\partial t} = \eta \frac{\partial^2 V}{\partial x^2} + G_V(V, W)$$
$$\frac{\partial W}{\partial t} = G_W(V, W)$$

where G_V and G_W are the right hand sides in (5a) and (5b) respectively.

After sufficient steps for the peak of the action potential to develop, the von-Neumann boundary conditions are replaced by periodic boundary conditions, which mimics a one-dimensional conducting ring along which an action potential travels.

When performing the simulation for different lengths, one finds several quantities of interest:

Base Cycle Length *BCL*, the time for the peak to travel along the line once (the time between two peaks, the period)

Conduction Velocity *CV*, Velocity of the peak (length of line divided by BCL)

Action Potential Duration *APD*, time between upstroke and downstroke

Rise Time duration of upstroke

Maximal Peak Height

These quantities were measured by monitoring a fixed point on the domain and checking at each time step whether the potential crossed either a low or a high threshold (5% and 95% of the maximal potential respectively). The length of the domain was varied between 25 and 200 and for each value 10 measurements were recorded by letting the peak pass through the domain 10 times after reaching a stable shape. Then average and standard deviation were computed and plotted (see fig. 7). For lengths below 25 the pulse can not sustain itself with the used parameters.

Of course, the BCL increases linearly with the maximal length. The CV and maximal peak height have smaller values for small lengths. With longer lengths those values first increase strongly in value

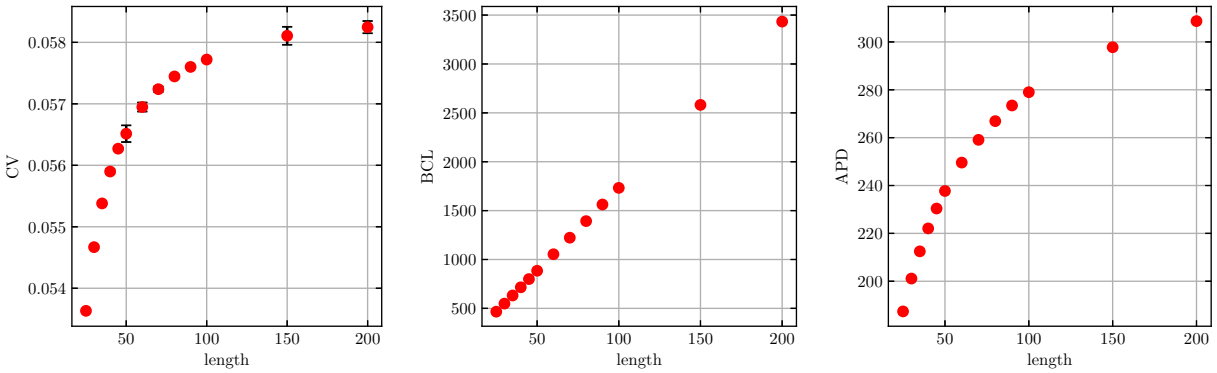

(a) conduction velocity (b) base cycle length (c) action potential duration

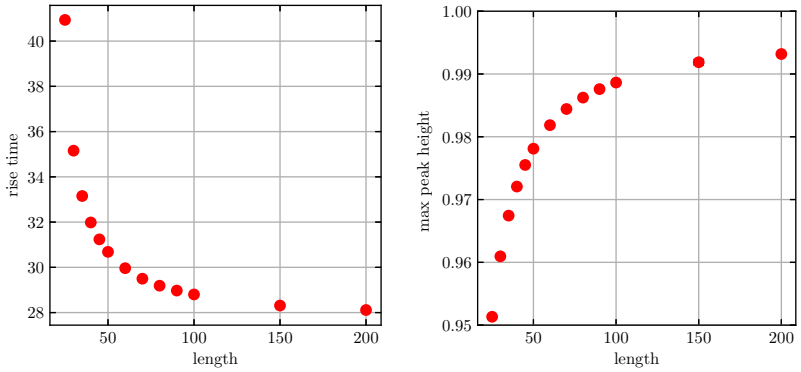

(d) rise time (e) max peak height

Figure 7: All measured quantities plotted against the domain length

and then seem to strive asymptotically against some upper limit (CV 0.0582, max peak: 0.9931). The APD seems to behave similarly, but to verify its asymptotic character, a closer investigation is required. The rise time is maximal for small lengths, then falls and goes towards some lower limit. One can conclude therefrom, that the action potentials rising edge is the most shallow for high rates and gets steeper for lower rates.

Concerning the theoretical estimated relationship between CV and rise time

$$CV \approx \sqrt{\frac{\eta}{2\tau}}(1 - 2\alpha) \tag{8}$$

the measured values were plotted in fig. 8 together with the curve given by (8) (where $\alpha = 0.17$ was obtained by fitting the measured data to the formula using a non-linear least squared method; this is justified, since α acts only as an offset).

In order to (naively) quantize this result, both curves were approximated as linear and a linear regression was computed (see table 1). The relative error of the slopes is ca. 48%.

	slope	r^2-value
measured	-3.7×10^{-4}	0.92
estimated	-7.7×10^{-4}	0.99

Table 1: Results of linear regression

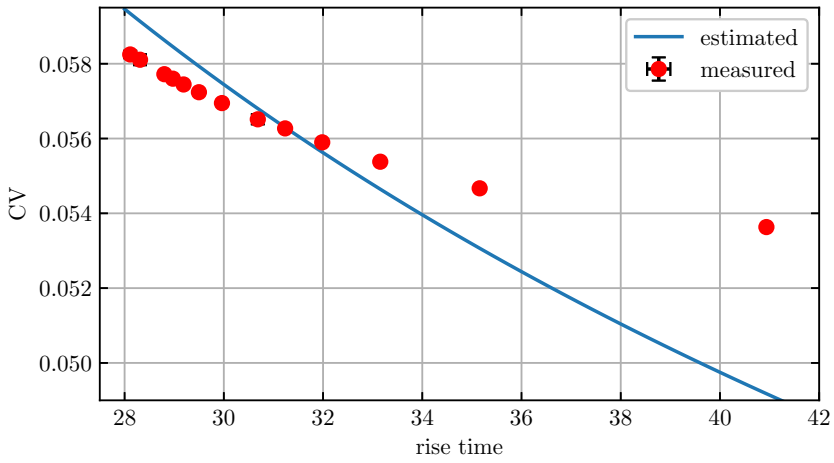

Figure 8: comparison of measurement and estimate

4.2. On a two-dimensional domain

The setups described below were simulated with the Aliev-Panfilov model and with the Fenton model. However hereafter only the results from the Fenton model are presented, since while exhibiting the same phenomena as the first-mentioned, it also shows some additional interesting features.

The Fenton simulation is based on three two-dimensional arrays holding the spatially resolved values of the membrane potential and the two inactivation gates. These arrays are update each time step with an Euler scheme according to

$$\begin{aligned}\frac{\partial V}{\partial t} &= \eta\,\nabla^2 V + G_V(V,v,w)\\ \frac{\partial v}{\partial t} &= G_v(V,v,w)\\ \frac{\partial w}{\partial t} &= G_w(V,v,w)\end{aligned}$$

where G_V, G_v and G_w are the right hand sides in (1), (6) and (7) respectively.

All of the following setups used grid steps $\Delta x = \Delta y = 1$. Varying this parameter corresponds simply to a rescaling of the system.

4.2.1. Channel

One considers a 64×256 grid with Dirichlet boundary conditions imposed along the long side (i. e. the x-direction) and periodic boundary conditions along the short side (i. e. the y-direction).

For the initial values of V and w the same narrow stripe (20 grid points wide) and for v a stripe of same width but shifted 10 grid points in positive x-direction were set to 1.

Running the simulation, an action potential quickly develps and repeatedly passes through the domain, which mimics a constant rate of pulses. Because of the Dirichlet conditions the action potential on the edges is pulled to zero, causing some kind of tail (see fig. 9).

4.2.2. Spiral Excitation

Now one considers a 128×512 grid with von-Neumann boundary conditions imposed on all sides. The initial conditions to generate the first pulse are the same as described above. Because of the boundary conditions, the pulse is not damped on the edges and passes through the domain only once.

Now a small area of 10×10 grid points right in the middle of the domain has its membrane potential set to 1. In the absence of any prior excitation this simply produces a circular pulse running away in all directions. But if this perturbation happens in the wake of a preceding action potential an interaction

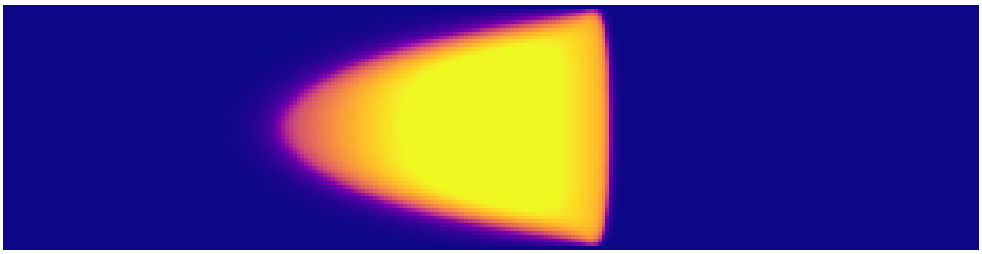

Figure 9: Pulse in channel setup

with the relaxation variables - which have not yet fully returned to their rest values - takes place: Either the perturbation is suppressed right away, or it is pushed backwards growing into the shape of an expanding croissant whose edges are running forward until they meet in the center. Upon this meeting the croissant becomes a pretzel which runs away in a circular fashion and the then slightly inwards turned edges generate a new croissant-shaped pulse which undergoes the same process.

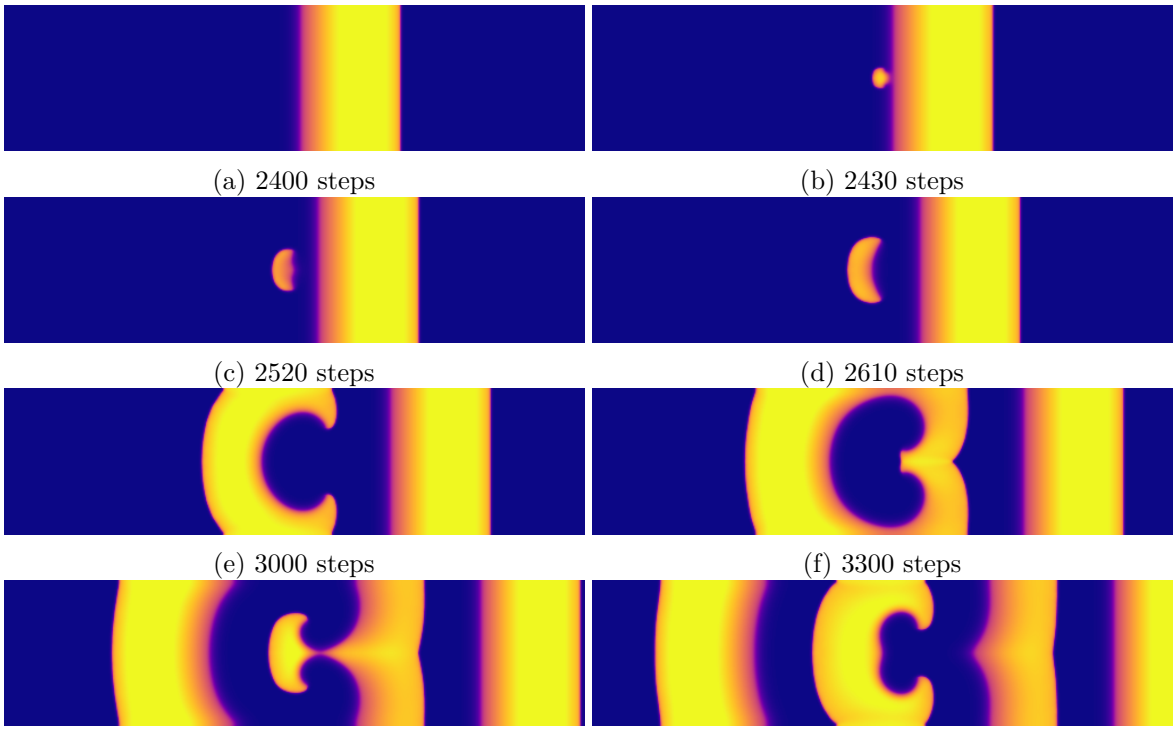

(a) 2400 steps (b) 2430 steps

(c) 2520 steps (d) 2610 steps

(e) 3000 steps (f) 3300 steps

(g) 3600 steps (h) 3900 steps

Figure 10: Image series of spiral excitation due to well-timed perturbation

For the given setup, the sweet spot in insert this perturbation lies around 2430 integration steps (see fig. 10).

While with the Fenton model each succeeding spiral is slightly damped causing the process to be extinguished completely after a finite number of iterations, the spirals generated with the Aliev-Panfilov model do not seem to exhibit such kind of behaviour and instead go on indefinitely.

4.2.3. Spiral Wave and Breakup

Finally one considers a 256×512 grid with von-Neumann boundary conditions on all sites. The initial conditions are given by a stripe of excited membrane potential which only reaches into the domain by some extend, i. e. it has a loose end.

When performing the simulation, the main part of the initial stripe develops into a pulse like seen before, but the loose end turns away growing into a spiral and eventually hits its own wake. When

the tip reaches not yet fully repolarized tissue, it fails to continue propagating normally and instead breaks up (in the Fenton model this is due to the interaction of the action potential of the tip with the inactivation gates in the wake). This process starts to successively generate new spirals. It amplifies itself, soon causing multiple spirals to be present at once, which spread out until the whole domain is disruptively filled with small and rather fast moving spirals (see fig. 11).

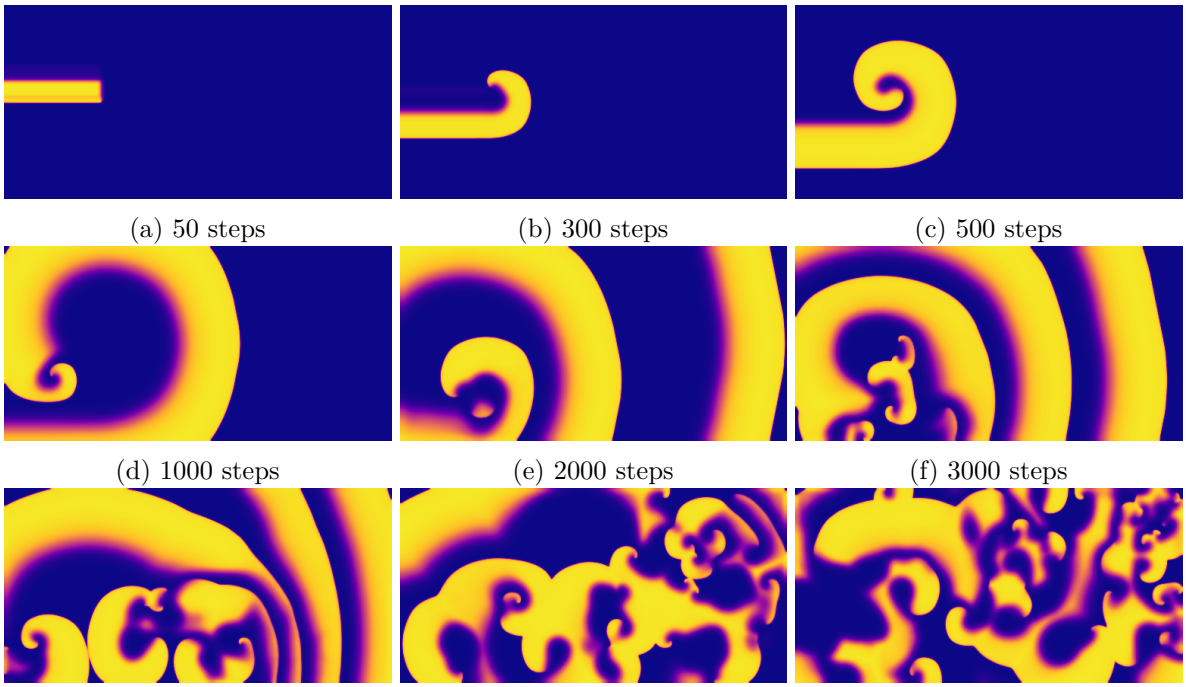

(a) 50 steps (b) 300 steps (c) 500 steps

(d) 1000 steps (e) 2000 steps (f) 3000 steps

(g) 4500 steps (h) 6000 steps (i) 7500 steps

Figure 11: Image series of spiral wave breakup due to tip-wake interaction

With the Aliev-Panfilov model the aforementioned initial conditions generate an ever-growing spiral without any disruptive behaviour.

5. Physiological Interpretation

5.1. One-dimensional ring

The one-dimensional ring described in section 4.1 can be interpreted as a conducting fibre of the hearts conduction system, through which a constant rate of action potentials passes. This rate can be varied by varying the length of the ring. While this approach seems rather simplistic, it can be used to understand the effects of tachycardia (i. e. abnormal high heart rates) on the characteristics of single action potentials: the peaks are more shallow (longer rise time), do not reach their full height, have a shorter duration and are being conducted somewhat slower.

Such deviations from the regular behaviour can express itself as arrhythmia and have a significant impact on the well-being of the affected person.

5.2. Channel

The situation depicted in section 4.2.1 of a confined channel could be used to describe a bundle of cells belonging to the electrical conducting system of the heart, which transmit action potentials at a constant rate to some target tissue area, in order to trigger its contraction.

While with the default configuration this mimics a properly working propagation of action potentials, one can also observe above described phenomena when shortening the length of the domain.

5.3. Spiral waves

In a healthy heart the action potential meant to trigger contraction is propagating homogeneously through the tissue. If now due to some pathological condition some regions in the cardiac tissue have different electrical conductivities or do not conduct at all (scar tissue), the action potential might travel around these obstacles eventually hitting its own wake and causing local depolarization deviating from the beat given by the SA node. Such phenomena are known as *re-entrant arrhythmia* and can cause ventricular tachycardia or atrial flutter and might develop into ventricular or atrial fibrillation. The only way to stop (the otherwise fatal) ventricular fibrillation is to apply a high energy electrically shock to depolarize all (or a critical mass) of cardiac tissue ($\rightarrow$ *defibrillation*). When the cells have repolarized, they can again be governed by the pace given by the SA node.

Such phenomena can be linked to action potentials spreading through the heart's tissue like spiral waves, which in reality occur due to heterogeneity of the tissue. On a simplified homogeneous domain, one can generate such configurations by choosing the initial conditions properly. The setups presented above achieve this by delivering a single impulse in the wake of a preceding action potential wave (see section 4.2.2) or by defining an initial wave with a loose end (see section 4.2.3). The spiral waves resulting from the first case and occurring in the beginning of the second case can be interpreted as ventricular tachycardia; the disruptive and uncoordinated behaviour eventually emerging from the second case resembles ventricular fibrillation evolving from preceding tachycardia (see also fig. 38 in [CH08]).

6. Discussion

6.1. The Models

6.1.1. Hodgkin & Huxley

The first-discussed model is very intuitive and gives a good understanding of the underlying process, since it is close to the physical background (even though the details were unknown at that time). Even hyperpolarization is included.

The results presented here were obtained with a time step of $\Delta t = 0.01\,\text{ms}$. Reasonable results were possible with larger time steps up to $\Delta t = 0.055\,\text{ms}$, however at this point the results already included artifacts due to numerical inaccuracies.

While the form of the action potential rather corresponds to neural cells and not cardiomyocytes, this could perhaps be achieved by fitting the parameters differently. The additional source current causing repeated depolarization can be used to describe permanently firing neurons or – with appropriate parameters – pacemaker cells in the SA node.

6.1.2. Aliev & Panfilov

While this model is rather difficult to interpret, since it is intended to only phenomenologically reproduce the observed dynamics, it allows one to perform larger spatial tissue simulations with reduced effort.

From this models simulation the measurements of the action potential properties for varying rate were recorded, which were compared to a theoretical estimate relating conduction velocity and rise time (8). While the gross form of the theoretical estimate and the measured data is similar, a rather clear deviation should be acknowledged. Quantitatively – from the compared slopes – a relative error of 48% is found. In order to make a clear statement whether the error is due to inaccuracies of the equation or of the used model, a more in-depth investigation would be needed.

6.1.3. Fenton et al

This model was introduced, because the previously discussed A&P model lacks the ability to depict more complex (and interesting) mechanisms. This comes with the price of a higher computational demand.

It is per se a phenomenological model, yet the used quantities (*currents* and *gates*) resemble the underlying physics closely. The parameters have physical meaning and are designed in such a way, that allows to influence the resulting behaviour purposefully.

6.2. Further Outlook

Throughout this work all simulations were performed with a simple Euler scheme. While this already gives meaningful results, one could alternatively apply more sophisticated ways such as a semi-implicit Crank-Nicolson scheme or multi-step Runge-Kutta methods. This would allow for larger time steps (making the simulations computationally cheaper) while maintaining accuracy.

It might be interesting to consider a heterogeneous domain, i. e. with anisotropic conductivity. One could investigate the behaviour of above discussed setups with a conductivity tensor resembling the structure of the myofibril. Such a simulation could be expanded to more complex geometries in order to describe fibre bundles of the conduction system or re-entrant waves due to scar tissue.

Further, developing solution methods for the bi-domain case would allow the investigation of the tissue's behaviour when subjected to external stimuli such as defibrillation.

A. Appendix

A.1. Varying the parameters of the Aliev & Panfilov model

Here is a quick study presented, which varies the parameters of the phenomenological Aliev-Panfilov model (5) and examines its behaviour: table 2 gives an overview including a description of the resulting change and in fig. 12 these changes were plotted.

Name	Range	Effect
a	0.1 to 0.2	• delay of V and W • $a = 0.2$: both variables are extinguished
k	4.0 to 14.0	• scaling strength and slope of W • the larger k, the faster and stronger rises W
ϵ_0	1×10^{-5} to 1.0	• makes W rise earlier • maintains the peak's shape
μ_1	0.05 to 2.0	• makes W rise earlier and steeper
μ_2	0.1 to 5.0	• delays W and flattens the peak

Table 2: Parameter overview

Literature

[CH08] E. M. Cherry and Fenton F. H. "Visualization of spiral and scroll waves in simulated and experimental cardiac tissue". In: *New Journal of Physics* (2008). DOI: 10.1088/1367-2630/10/12/125016.

[Cla+11] R.H. Clayton et al. "Models of cardiac tissue electrophysiology: Progress, challenges and open questions". In: *Progress in Biophysics and Molecular Biology* (2011). DOI: 10.1016/j.pbiomolbio.2010.05.008.

[Dre17] Jürgen Dreher. *Numerical Simulation of Cardiac Tissue Electrophysiology. Versuchsanleitung zum Fortgeschrittenen-Praktikum.* Ruhr-Universität Bochum. 2017.

[FCG08] F. H Fenton, E. M. Cherry, and L. Glass. "Cardiac arrhythmia". In: *Scholarpedia* 3.7 (2008). revision #121399. DOI: 10.4249/scholarpedia.1665.

[Fen+02] Flavio H. Fenton et al. "Multiple mechanisms of spiral wave breakup in a model of cardiac electrical activity". In: *Chaos: An Interdisciplinary Journal of Nonlinear Science* (2002). DOI: 10.1063/1.1504242.

[HH52] A. L. Hodgkin and A. F. Huxley. "A quantitative description of membrane current and its application to conduction and excitation in nerve". In: *The Journal of Physiology* (1952). DOI: 10.1113/jphysiol.1952.sp004764.

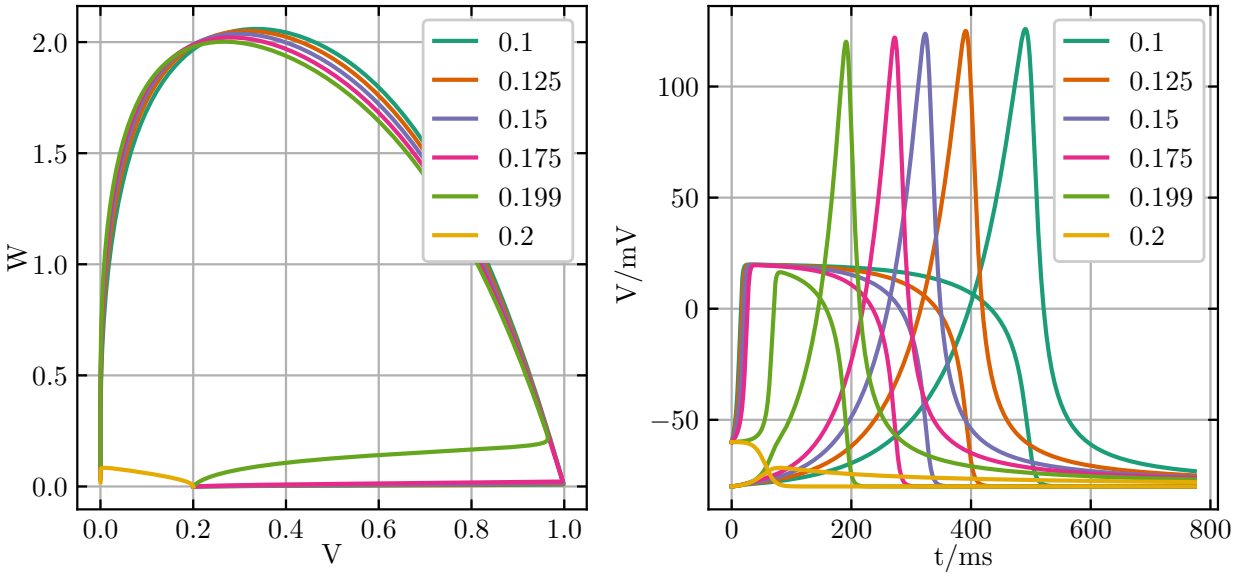

(a) a

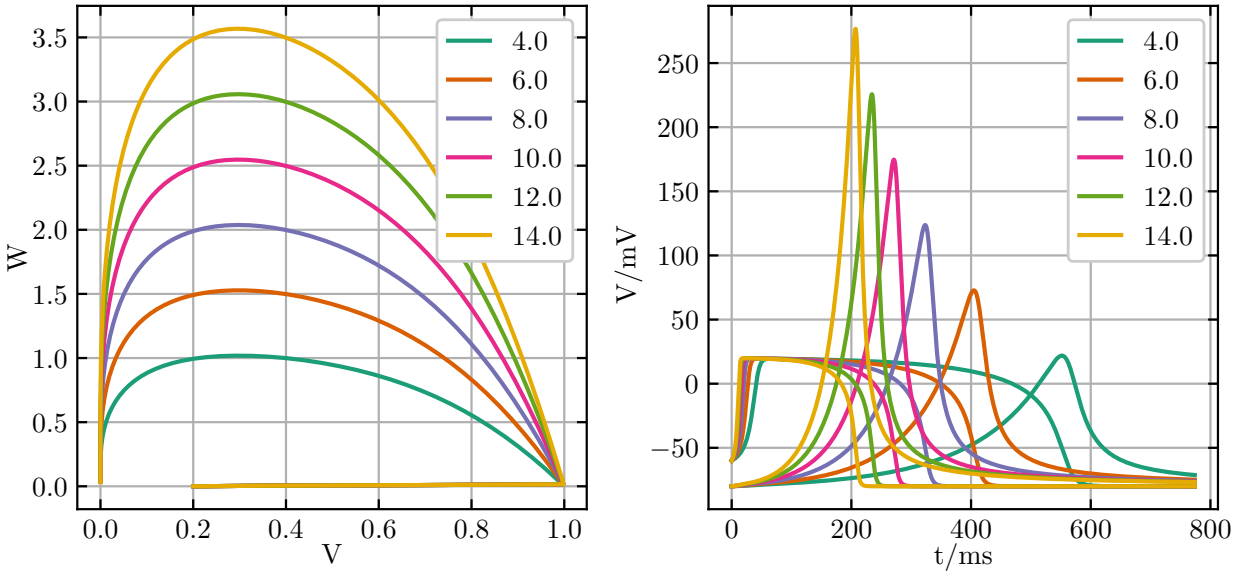

(b) k

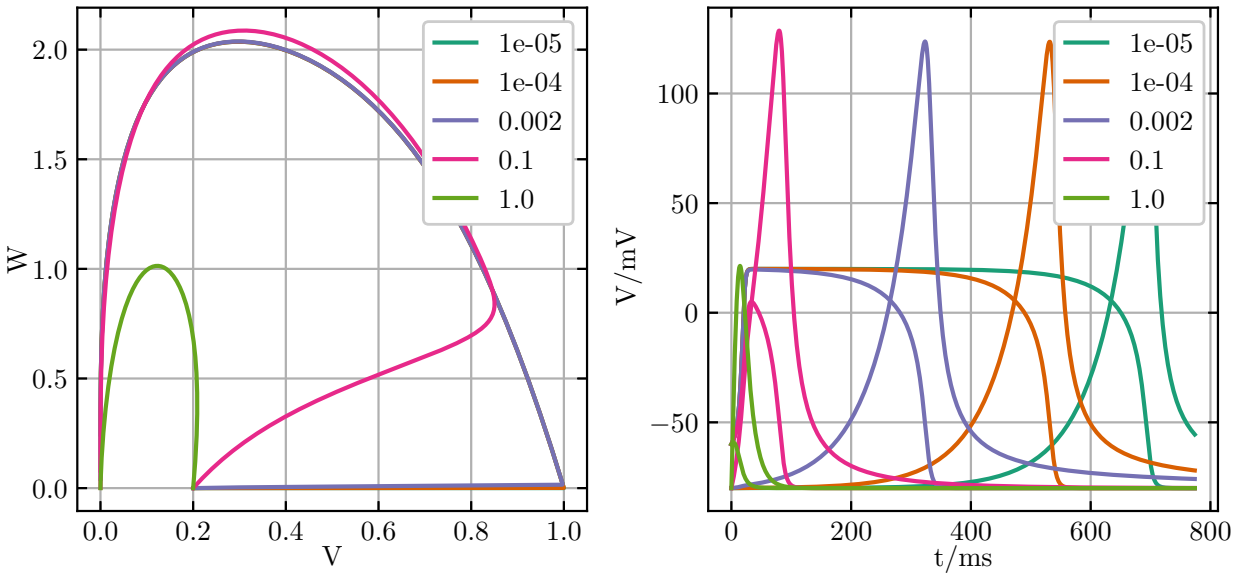

(c) ϵ_0

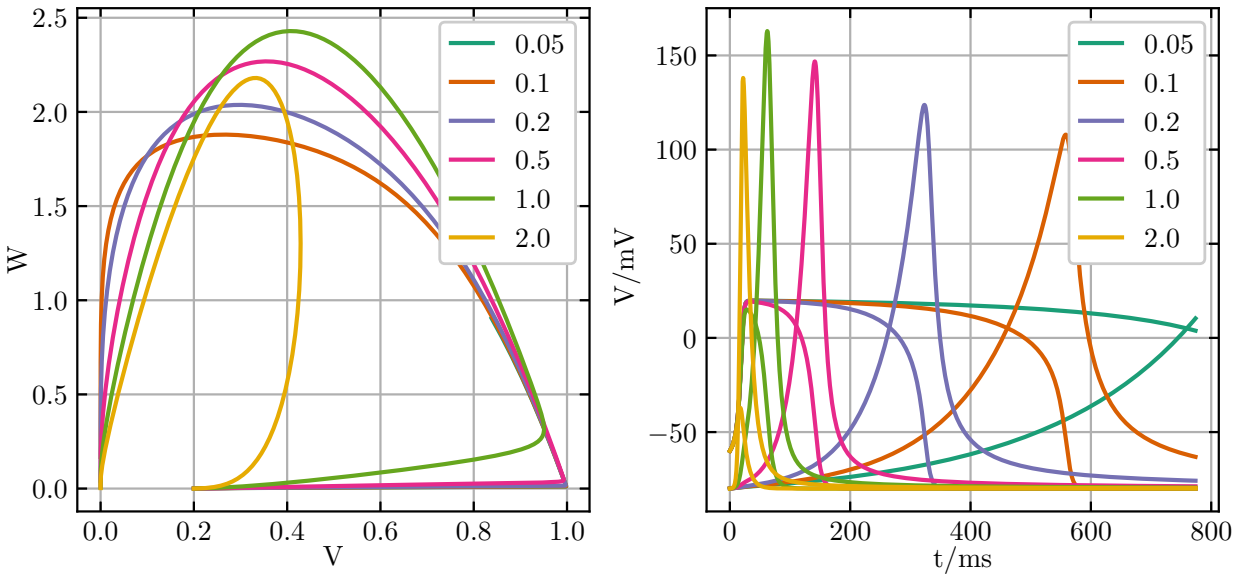

(d) μ_1

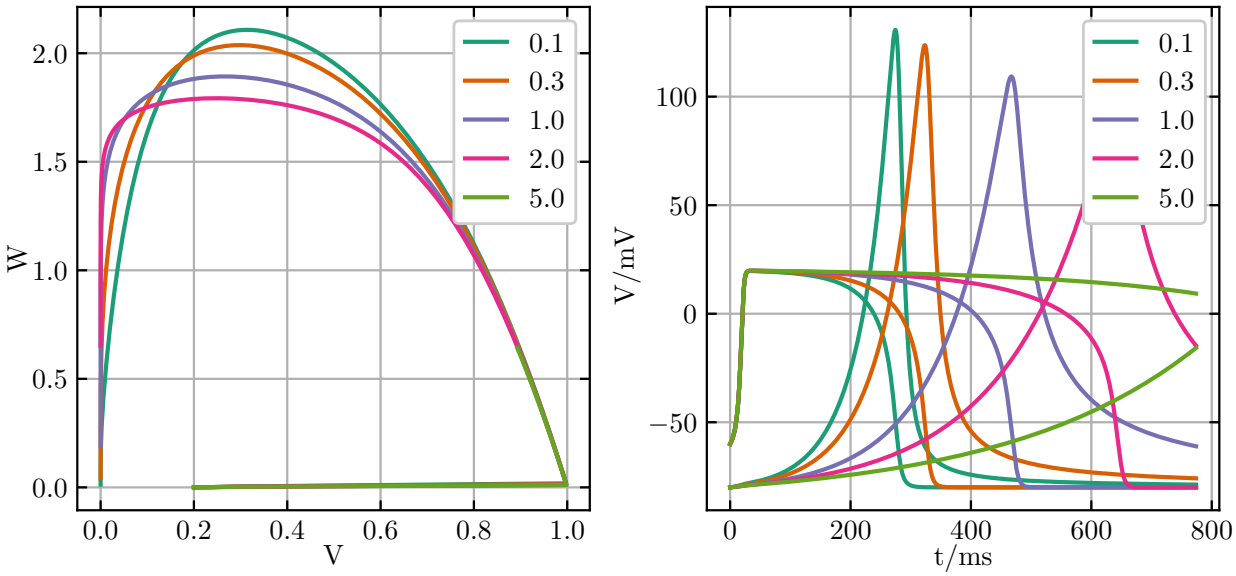

(e) μ_2

Figure 12: Plots for varying parameters